A Global Sensitivity Analysis Study with More Parameters in Undermoded Reverberation Chambers

Anett Kenderes*† , Szabolcs Gyimóthy*, and Péter T. Benkő†

*Department of Broadband Infocommunications and Electromagnetic Theory,
Budapest University of Technology and Economics, Műegyetem rkp. 3., H-1111 Budapest, Hungary
† Automotive Electronics – Electromagnetic Compatibility (AE/EMC-HU)
Robert Bosch Kft., Gyömrői út 104., H-1103 Budapest, Hungary
E-mail: kenderes.anett@edu.bme.hu

***Abstract*—An improved global sensitivity analysis (SA) study by means of Sobol' indices was performed in this work to investigate the influence of measurement uncertainties on an adequately chosen quantity, which describes the field distribution in the stochastic environment of reverberation chambers (RC). A kriging metamodel is utilized to substitute the computationally expensive full-wave simulation model of a certain RC. This black-box approach provides an efficient apparatus for the stirring and chamber design process.**

***Index Terms*—reverberation chambers, sensitivity analysis, surrogate modeling, electromagnetic simulation**

I. Introduction

RCs provide a versatile tool for measurements in which an environment with stochastic field properties should be established [1]. Besides the acoustical regime, it becomes a more and more important facility in the electromagnetic (EM) range. A non-exhaustive list of the possible measurement types that can be performed in an RC consists of the electromagnetic compatibility (EMC) measurements, such as radiated immunity (RIA), radiated emission (REA), and shielding efficiency (SE), as well as over-the-air (OTA) tests in wireless communication, and biomedical investigations. This enclosure imitates the stochastic EM illumination of a real-world environment better compared to the common approaches like anechoic chambers (AC) and TEM-cells, exposing certain equipment under test (EUT) with an omnidirectional field illumination.

To achieve the aforementioned stochasticity, the deterministic behaviour of the highly resonant field distribution could be modified in several ways by slightly displacing the eigenfrequencies. To this end, the research tendencies shifted to less space-consuming solutions [2], such as source and frequency stirring, as well as vibrating intrinsic RC (VIRC). However, the most traditional technique, namely mechanical stirring [1], still plays a crucial role in the automotive industry.

The main benefit of establishing such an environment is the significant increase in the setup-based reproducibility of the measurement compared to the conventional methods. Nonetheless, there exist cases which need further investigation due to the inevitable nonidealities. A profound inspection of multiple setup parameters such as stirrer position, geometry, antenna position and orientation etc., is still a hot topic [4]-[13]. An extensive literature review can be read in [14].

Some attempts were made to introduce global SA methods [15] to the field of EMC measurements performed in ACs, e.g., [16] [17], in which the powerfulness of these techniques is unquestionable. The main contribution of [14] was the extension of the application area of the method of Sobol' indices [18] to RCs. This work considers further parameters, which yields a tool for more profound investigations. The corresponding parameters of the stirrer and the antenna are taken as input parameters of this black-box model, while the composite quality factor (Q-factor) is utilized as an output value.

II. Field distribution models in RCs

The statistical properties derived from the theory of plane wave expansion of the underlying phenomena were thoroughly investigated in [19], in which the theoretical considerations serve as a basis of the automotive standards, e.g., [3] [20]. Since then, several other attempts were made for further improvements [4] [5]. Besides, there exist other approaches e.g., in which the corresponding expressions are obtained by performing modal expansion [4] [21].

The heart of the assumption introduced in [19] is that there are an infinite number of propagating plane wave components in a source-free region, which yields a continuous spectrum along the solid angle. These premises are asymptotically fulfilled for electrically large RCs with a high amount of occupied working volume (WV). The resultant plane wave integral representation reads

$$\vec{E}(\vec{r}) = \iint_{4\pi} \vec{F}(\vec{r})\, e^{-j\vec{k}\cdot\vec{r}}\, \mathrm{d}\Omega, \tag{1}$$

where $\vec{F}$ is the angular spectrum, $\vec{k}$ is the vector wavenumber, and Ω is the solid angle. If the solid angle is defined as $\mathrm{d}\Omega = \mathrm{d}\sin\vartheta\ \mathrm{d}\vartheta\ \mathrm{d}\varphi$, the following expression can be obtained for the vector wave number

$$\vec{k} = k(\hat{x}\sin\vartheta\cos\varphi + \hat{y}\sin\vartheta\sin\varphi + \hat{z}\cos\vartheta), \tag{2}$$

https://doi.org/10.3311/WINS2023-008

where ϑ and φ denote the elevation and azimuth angles in a spherical coordinate system, respectively.

The isotropic property of the electric field implies that the mean-square of each component is equal and independent of the position. A direct consequence is that real and imaginary parts of the rectangular components follow Gaussian distribution. The magnitude of each component follows Rayleigh distribution, while in the case of imperfect stirring, Rice, Weilbull or generalized extreme value (GEV) distributions provide suitable alternatives under certain conditions [1].

The governing treatment of this problem is under the auspices of the statistical regime by performing Monte Carlo simulations (MC). Notwithstanding, electromagnetic modeling is inevitable in many applications when the physical extent and properties of the chamber, the instruments, and the EUT play an important role, like the aforementioned stirrer design process. Full-wave simulation might be essential, especially when parallelization is performed while carrying out RIA measurements of different EUTs simultaneously, and the setup should be adapted to the decreased WV. The modeling of RCs was investigated during the past decades from quite different perspectives and applications utilizing a vast of popular numerical methods such as finite element method (FEM), integral equations (IE), finite-difference time-domain method (FDTD), geometrical optics (GO), and transmission line method (TLM) [1].

A SA comes into play in the lower frequency range, where the ideal properties cannot be established, thus the importance of the physical parameters can vary from configuration to configuration. In the well-stirred case, all the parameters should have the same, low significance. However, there is no unequivocal agreement for the lowest usable frequency (LUF), where the field is well-stirred, the overmoded condition applies, thus the RC is capable of performing certain test [22]. The most common thumb rules considered in this work are listed in [14].

III. Methodology

A. Global SA

Let $\mathcal{M}(\boldsymbol{x})$ be a mathematical model, depending on a set of input variables formed in a parameter vector $\boldsymbol{x}$, which was scaled to the $[0,1]$ interval beforehand. A vast of SA techniques can be used to reveal the effects of adequately chosen parameters to the output vector $\boldsymbol{Y} = \mathcal{M}(\boldsymbol{x})$, and additionally, to spot unimportant ones based on this black-box approach [15]. The nature of the problem made us the choice to a candidate of global SA methods, namely the aforementioned Sobol' indices calculation [18] due to its robustness [15]. A more detailed explanation is included in [14].

The Sobol' indices [18] aim to represent the single and the overall contribution of each input variable. The construction is based on the decomposition of the output variance into individual variances and subvariances if the distribution of $\boldsymbol{x}$ is known *a priori*. By normalization, one can obtain the first-order and the total Sobol' indices of each parameter vector component, respectively

$$S_i = \frac{D_i}{D}, \quad ST_i = \frac{D_i + \sum_{i<j}^{n} D_{ij} + \cdots + D_{1,\ldots n}}{D}, \tag{3}$$

which correspond to the ith variable. The indices are scaled to the $[0,1]$ interval. D and $D_{1,\ldots n}$ denote the total and the partial variances, respectively.

B. The Utilized Metalmodel

In order to acquire a more cost-efficient model to calculate these indices, the true simulator is substituted by a functional approximation

$$\mathcal{M}(\boldsymbol{x}) \approx \mathcal{M}^{\text{Meta}}(\boldsymbol{x}). \tag{4}$$

In [14] paper, three state-of-the-art approaches were examined, out of which the stochastical perspective of the so-called kriging model appeared to be the most suitable resulting from the highly resonant and fluctuating behaviour of the RC.

The kriging metamodel [15] constructs the model output as a realization of a Gaussian process, which can be described by the following equation

$$\mathcal{M}^{\text{K}}(\boldsymbol{x}) = \boldsymbol{\beta}^T \boldsymbol{f}(\boldsymbol{x}) + \sigma^2 Z(\boldsymbol{x}, W), \tag{5}$$

where the first term is the trend, i.e., the mean value of the Gaussian process, consisting of the linear combination of known $\boldsymbol{f}(\boldsymbol{x})$ basis functions, e.g., polynomials, and the second term is a multiplication of the variance of the Gaussian process σ^2 and a zero-mean, unit-variance stationary Gaussian process $Z(\boldsymbol{x}, W)$. The underlying probability space is represented by W and defined in terms of a correlation function, i.e., a correlation family $R(\boldsymbol{x}, \boldsymbol{x}', \boldsymbol{\theta})$. This quantity describes the correlation between two sample points in the output space, which is not known *a priori*, thus it should be estimated using the existing data. The most common choice for this purpose is the Matérn covariance function due to its flexible tuning properties under the assumption of a stationary process depending only on the distance between the observations $h = |\boldsymbol{x} - \boldsymbol{x}'|$ as follows

$$R(h) = \frac{\sigma^2}{2^{\nu-1}\Gamma(\nu)} \left(2\sqrt{\nu}\frac{h}{\rho}\right)^{\nu} \mathcal{K}_{\nu}\left(2\sqrt{\nu}\frac{h}{\rho}\right), \tag{6}$$

where σ^2, ν, and ρ are the hyperparameters, the empirical sample variance, the regularity, and the range, respectively, usually summarized in a vector for the sake of brevity $\boldsymbol{\theta} = \{\sigma^2, \nu, \rho\}$, Γ is the Gamma function, and $\mathcal{K}_{\nu}$ is the modified Bessel function of the second kind. In [14] the simplified version of this expression was used with one of the most frequent choices of $\nu = 5/2$, which is denoted by Matérn-$5/2$. The hyperparameter estimation is usually performed by the maximum likelihood (ML) method or LOO error cross-validation (CV).

C. Error calculation

For validation purposes, the same error calculation is used in this work as in [14], which is based on the approximation of the relative generalization error. This measure quantifies the accuracy and predictive quality of the metamodel and defined as [15]

$$\epsilon_{\text{gen}} = \frac{\mathbb{E}\left[\mathcal{M}(\boldsymbol{X}) - \mathcal{M}^{\text{Meta}}(\boldsymbol{X})\right]}{\text{Var}[Y]}, \tag{7}$$

where $\mathcal{M}^{\text{Meta}}(\boldsymbol{X}) = \mathcal{M}^{\text{K}}(\boldsymbol{X})$ in this case.

The validation error is practical when besides the training set, there is a possibility of the construction of a validation set independently, the validation error can be calculated, which is defined by the following formula [15]

$$\epsilon_{\text{Val}} = \frac{N-1}{N} \frac{\sum_{i=1}^{N} \left(\mathcal{M}\left(\boldsymbol{x}_{\text{Val}}^{(i)}\right) - \mathcal{M}^{\text{Meta}}\left(\boldsymbol{x}_{\text{Val}}{}^{(i)}\right)\right)^2}{\sum_{i=1}^{N} (\mathcal{M}(\boldsymbol{x}_{\text{Val}}^{(i)}) - \hat{\mu}_{Y_{\text{Val}}})^2}, \tag{8}$$

where $\hat{\mu}_{Y_{\text{Val}}}$ is the sample mean of the validation set response calculated as

$$\hat{\mu}_{Y_{\text{Val}}} = \frac{1}{N} \sum_{i=1}^{N} \mathcal{M}\left(\boldsymbol{x}_{\text{Val}}{}^{(i)}\right). \tag{9}$$

If no validation set is available due to the computational expense of the physical model, as an alternative, the leave-one-out (LOO) cross-validation error can be utilized as [15]

$$\epsilon_{\text{LOO}} = \frac{\sum_{i=1}^{N} \left(\mathcal{M}\left(\boldsymbol{x}^{(i)}\right) - \mathcal{M}^{\text{Meta}\setminus i}\left(\boldsymbol{x}^{(i)}\right)\right)^2}{\sum_{i=1}^{N} (\mathcal{M}(\boldsymbol{x}^{(i)}) - \hat{\mu}_Y)^2}, \tag{10}$$

where $\hat{\mu}_Y$ is the sample mean of the experimental design response

$$\hat{\mu}_Y = \frac{1}{N} \sum_{i=1}^{N} \mathcal{M}\left(\boldsymbol{x}^{(i)}\right). \tag{11}$$

Due to the relatively high computational complexity, as in [14], we restrict ourselves to rely on the LOO error instead of the validation error.

IV. Building up the Metamodel

A. The Computational Model

As in [14], a FEM model built via the commercial CST simulation software is used for the SA study. As it has already been clarified in [14], it is more straightforward to use a model built in a commercial software framework for automotive applications. Nevertheless, the calculations can be obviously accelerated for special cases by numerical techniques such as parallel computing in [10]. The RC in this numerical example has sizes of $7.3\,\text{m} \times 5.5\,\text{m} \times 4.5\,\text{m}$. The simulations are carried out again at $100\,\text{MHz}$, around the estimated lowest usable frequency of this RC. The fundamental resonance has already been calculated by the Eigenmode Solver tool of the software in [14] and appeared to be at $f_0 \approx 34\,\text{MHz}$. At this frequency, imperfect stirring is expected, which yields higher importance that can be addressed to certain parameters, i.e., higher Sobol' indices. The stirrer design is the same as in [14], a common Z-shaped with dimensions set by a thumb rule stated in [1]. The stirrer volume is 8.3% of the RC volume, which approximates the minimum volume mentioned in [1]. The angles of the blades were set initially uniformly to $\alpha = 40°$. The TX antenna was chosen to be a dipole antenna, designed for the test frequency for the sake of reducing the computational complexity of modeling the most commonly used log-periodic antenna as in [28]. The TX antenna points to the furthermost corner with respect to the location of the stirrer and the WV, as suggested in the standards [3][20][27]. In order to cover the worst-case scenario in the sense of occupied WVs with the proximity of metallic surfaces, the maximum WV is investigated as depicted below in Fig. 1 at $\lambda_{\text{test}}/4$ distance from each conductive surface in the RC, which is specified as a minimum distance in the standards [3][20]. (The military standards set a more stringent requirement of $\lambda_{\text{test}}/3$ [27]). λ_{test} denotes the lowest frequency of use.

B. Input Parameters

The input parameters were chosen again to look into the $\pm 10\%$ setup uncertainties with respect to the recommendations and requirements of the [3] standard as it is usually done in uncertainty quantification (UQ) studies, e.g., [16], but with an extended parameter set. The input parameter descriptions are listed in Tab. I, and the ranges of inspection are detailed in Tab. II. In this study, additional spacial displacements and the modification of the angles of the stirrer blades are investigated as well. The neglection of the spatial displacement $\Delta_{y_{\text{stirrer}}}$ was due to the configuration being slightly modified compared to [14], in which it is impossible to apply a displacement of the stirrer along the y axis without violating the aforementioned $\lambda/4$ condition, meanwhile the input parameter set corresponding to the TX antenna could be extended. In Fig. 1, the parameters related to the TX antenna are marked in blue, and the red colour is assosiated with the stirrer-related ones.

Parameter	Description
φ_{TX} [deg]	orientation of the TX antenna in azimuth direction
ϑ_{TX} [deg]	orientation of the TX antenna in elevation direction
$\Delta_{x_{\text{TX}}}$ [cm]	displacement of the TX antenna along the x axis
$\Delta_{y_{\text{TX}}}$ [cm]	displacement of the TX antenna along the y axis
$\Delta_{z_{\text{TX}}}$ [cm]	displacement of the TX antenna along the z axis
$\Delta_{x_{\text{stirrer}}}$ [cm]	displacement of the stirrer along the x axis
$\Delta_{z_{\text{stirrer}}}$ [cm]	displacement of the stirrer along the y axis
$\alpha 1_{\text{stirrer}}$ [deg]	angle between the 1st and the 2nd blades of the stirrer
$\alpha 2_{\text{stirrer}}$ [deg]	angle between the 2nd and the 3rd blades of the stirrer
$\alpha 3_{\text{stirrer}}$ [deg]	angle between the 3rd and the 4th blades of the stirrer

TABLE I: The intervals of the input parameters

C. Output Parameters

The most traditional way to quantify the field uniformity, in other words, the ideal properties of RCs is to

Input parameter	Interval
φ_{TX} [deg]	$[288, 352]$
ϑ_{TX} [deg]	$[63, 87]$
$\Delta_{x_{\mathrm{TX}}}$ [cm]	$[-10, 10]$
$\Delta_{y_{\mathrm{TX}}}$ [cm]	$[-10, 10]$
$\Delta_{z_{\mathrm{TX}}}$ [cm]	$[-10, 10]$
$\Delta_{x_{\mathrm{stirrer}}}$ [cm]	$[-10, 10]$
$\Delta_{z_{\mathrm{stirrer}}}$ [cm]	$[-10, 10]$
$\alpha 1_{\mathrm{stirrer}}$ [deg]	$[36, 44]$
$\alpha 2_{\mathrm{stirrer}}$ [deg]	$[36, 44]$
$\alpha 3_{\mathrm{stirrer}}$ [deg]	$[36, 44]$

TABLE II: The intervals of the input parameters

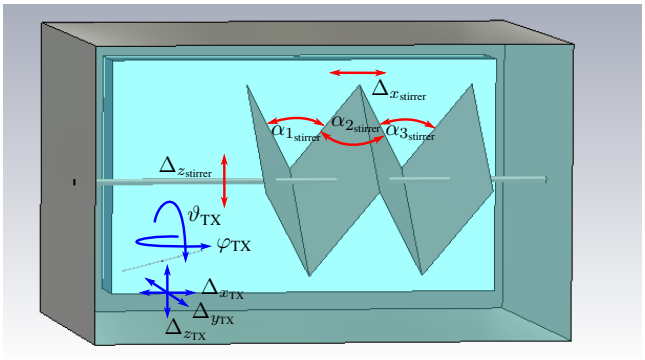

Fig. 1: The input parameters and the WV used for the SA

calculate the standard deviations (SD) specified in the standards as a SD from the mean value of the maximum values normalized to the TX power, obtained from each of the probes placed at the corners of the WV during all stirring configurations. The SD is calculated using data from each probe axis independently and the total data set. The obtained values shall be expressed in terms of dB relative to the mean as follows [3][20][27]

$$\sigma_i \text{ [dB]} = 20 \log \left(\frac{\sigma_i + \langle e_i \rangle}{\langle e_i \rangle} \right), \quad i = \{x, y, z\}, \tag{12}$$

$$\sigma \text{ [dB]} = 20 \log \left(\frac{\sigma + \langle e \rangle}{\langle e \rangle} \right). \tag{13}$$

As in the previous paper [14], the quality factor (Q-factor) was chosen as the output parameter for the SA. Out of a decent number of parameters to characterize the statistical properties of RCs, the Q-factor is claimed to be one of the most stable ones [31]. Indeed, it was more suitable for the application of the kriging metamodel than the SDs specified in the standards [3][20][27] by its nature being a purely physical integral quantity without any restrictions providing a slightly smoother output function than the SDs. In the case of the SD calculation, oversampling the domain with field probes can cause violation of the sample independence condition in terms of the coherence cells (ideally, cubes with a volume of $(\lambda/2)^3$ [7]).

The Q-factor is the ratio of energy stored to the energy dissipated per cycle in a resonator

$$Q = \frac{\frac{1}{2}\,\omega\varepsilon \int_0^a \int_0^b \int_0^c |E|^2 \,\mathrm{d}x\,\mathrm{d}y\,\mathrm{d}z}{P_{\mathrm{d}}}, \tag{14}$$

where ω is the angular test frequency, ε is the permittivity of the air (or equivalent medium), $|E|$ is the magnitude of the E-field, and P_{d} is the average dissipated power in a period. This quantity includes the chamber losses. In addition, it is related to the time constant, and the characteristic bandwidth of the RC [19]. Thus, the Q-factor have primary importance in the RC design process. Since each eigenmode is linked to a Q-factor, it is more desirable to define the composite Q-factor, which describes the chamber as a whole

$$\hat{Q} = \frac{1}{2}\,\omega\varepsilon \int_0^a \int_0^b \int_0^c \langle \bar{E} \rangle^2 \,\mathrm{d}x\,\mathrm{d}y\,\mathrm{d}z, \tag{15}$$

where $\langle \bar{E} \rangle$ is the average electric field magnitude normalized with the TX power over the stirrer rotation under energy conservation condition. The formula in (15) can be approximated as follows under well-stirred condition, which yields the simplification of the volume integral due to the isotropic field properties and even provides a fair estimation in the lower frequency range to some extent [28]

$$\hat{Q} \approx \frac{1}{2}\omega\varepsilon V \langle \tilde{E} \rangle^2, \tag{16}$$

where V is the chamber volume, and $\langle \tilde{E} \rangle^2$ is the total average of $\langle \bar{E} \rangle$ over all stirrer rotations and sampling positions, as it is done while calculating the SD in the standards [3][20][27]. The only difference is that it is not necessary to take the maximum values of each quantity measured by the field probes. The desired accuracy in most practical applications is even achievable for a reduced number of stirrer positions or field probes, depending on the nature of the experimental or numerical approaches. In our case, using the already generated data for the SD evaluation is more evident. However, in order to smoothen the fluctuating behaviour of the Q-factor, which is due to the nature of the RC environment, and additionally, to provide a more suitable approximation for the volume integral in (15), further field probes are added to the simulation setup with an amount of $9 \times 4 \times 6$ along the $x, y,$ and z axes, respectively, which yielded 216 sampling points, where the magnitude of the E-field, and the x, y, z components were monitored. Besides, as in [14], it was more favourable to normalize with the actual input power instead of an average value over the stirrer rotation suggested in the standards [3][20]. It is worth mentioning that there exist other approaches for the composite quality factor derived from ideality considerations [19][31].

V. Results

The applicability of the RC from 100 MHz to 200 MHz in terms of the SD requirements [3] have already been checked in [14]. The criteria passed at 12 rotational steps in stepwise operation of the stirrer, which is the minimum value specified for the frequency range of $f_{\mathrm{LUF}} \ldots 3 f_{\mathrm{LUF}}$.

The numerical instabilities yielded from the highly resonant behaviour were handled by introducing a fictive

conductivity of 10^{-5} S/m for the air, which implies approximately equivalent lossy behaviour as utilizing aluminium walls with lossless internal medium changing the statistical properties only moderately [28]. This yielded a more stable model than the conventional one during a mesh refinement convergence study.

The total simulation time with the FEM-solver for 200 experimental design (ED) samples, i.e., the $\{\boldsymbol{x}, \mathcal{M}(\boldsymbol{x})\}$ pairs obtained by latin hypercube sampling (LHS) [15] took a week using a computer with i7 processor. The overall number of required simulations was $N_{\text{st}} \cdot N_{\text{s}} = 2400$, where N_{st} and N_{s} denotes the number of stirring steps and experimental design samples, respectively. Despite the fact that the number of samples was doubled, the more than twice time consumption is owing to the enlarged number of field probes, resulting in an increased amount of post-processing steps. The memory consumption was about 3 GB. The number of mesh elements was 125k on average. The data were post-processed via MATLAB to calculate the corresponding Q-factors of each ED sample. he SA was carried out using the UQLab Toolbox [15] in MATLAB framework. The LOO error was 9.5% in this study, which is addressed to the significantly extended input parameter range. This result seems to be promising, though a convergence study with respect to the LOO error should be carried out in the future.

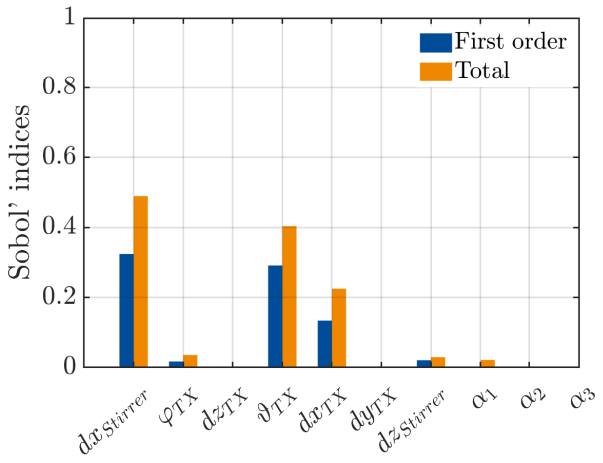

Fig. 2: The Sobol' indices obtained for the Q-factor

VI. Conclusion

In this measurement configuration, again, the elevation angle of the TX antenna and the displacement of the stirrer along the x direction have the highest single-order Sobol' indices, i.e., the highest single significance as it is depicted in Fig. 2, which have been already discussed in [14]. One major conclusion of the extended SA is that the parameters contributing to the EM coupling between the TX antenna and the stirrer have higher Sobol' indices, which implies that this phenomenon is the most dominant in the lower frequency range. Surprisingly, the importance of the variation of the angles between the blades appeared to be not remarkable compared to the other investigated parameters despite the vast of previous attempts that can be found in the literature to investigate its effect on the FU. However, higher variations and their frequency-dependent behaviour should be inspected in the future. The total Sobol' index of α_1 is relatively distinguishable because of the proximity of the stirrer.

Further investigations will include cases when the effects of the stirrer or the antenna illumination are dominant. The examinations will be extended to a numerically reasonable frequency range by using further surrogate modeling techniques such as adaptive sampling involving a kriging or PCK metamodel to reduce the required frequency sample points similarly to [29]. Other parameters are to be studied as well, such as stirring and RC volume. Different stirrer orientations, geometries and antenna types should be tried out as well. A wider parameter range is also to be inspected, where the worst cases in the test setup could be involved. These scenarios should be handled differently because dependence occurs between the variables, which would cause the non-applicability of Sobol' indices. The limits of the pertinence should be checked first. Alternatively, extended Sobol' indices based on covariance decomposition can be used. Finally, a SA study considering the SD measures should be performed while finding a way to smoothen the fluctuating behaviour of these quantities without violating the aforementioned sample independence conditions. The complete analysis might serve as a basis for setup adaptation during parallelized EMC tests, which yields a more time and cost-saving option in industrial applications. In addition, some extra conclusions may be drawn in terms of the frequency-dependent behaviour of each parameter via a global SA study.

VII. Acknowledgement

The reported research has been carried out with the professional support of the Doctoral Student Scholarship Program, which was under the auspices of the Co-Operative Doctoral Program of the Ministry for Innovation and Technology from the source of the National Research Development and Innovation Fund. Furthermore, this work was supported by the Hungarian Scientific Research Fund under grant K-135307.

References

[1] Q. Xu, Y. Huang, Anechoic and Reverberation Chambers: Theory, Design, and Measurements, John Wiley & Sons, 2019.

[2] Z. Tian, Y. Huang, Y. Shen, and Q. Xu , "An electrical stirring method for a reverberation chamber," in *2014 Loughborough Antennas and Propagation Conference (LAPC)*, pp. 236-238, IEEE, November 2014.

[3] ISO 11452-11, Road vehicles — Component test methods for electrical disturbances from narrowband radiated electromagnetic energy — Part 11: Reverberation chamber, 2010.

[4] A. Cozza, "The Role of Losses in the Definition of the Overmoded Condition for Reverberation Chambers and Their Statistics ," in *IEEE Transactions on Electromagnetic Compatibility*, vol. 53. 2, pp. 296–307, 2010.

[5] R. J. Pirkl, K. A. Remley, C. S. L. Patane, "Reverberation Chamber Measurement Correlation ," in *IEEE Transactions on Electromagnetic Compatibility*, vol. 54.3, pp. 533–545, 2011.
[6] C. Cammin, T. Doebbert and G. Scholl, "Influence of Stirrer Vibration During Stepwise Operation of a Reverberation Chamber," in *2022 16th European Conference on Antennas and Propagation (EuCAP)*, pp. 1-5, 2022.
[7] L. R. Arnaut, "Effect of size, orientation, and eccentricity of mode stirrers on their performance in reverberation chambers," in *IEEE Transactions on Electromagnetic Compatibility* Vol. 48 No. 3, pp. 600-602, 2006.
[8] V. M. Primiani and F. Moglie, "Reverberation Chamber Performance Varying the Position of the Stirrer Rotation Axis," in *IEEE Transactions on Electromagnetic Compatibility*, vol. 56.2, pp. 486-489, 2014.
[9] O. Lundén, N. Wellander, and M. Bäckström, "Stirrer blade separation experiment in reverberation chambers," in *2010 IEEE International Symposium on Electromagnetic Compatibility*, 2010.
[10] G. Bosco, C. Picciani, V. M. Primiani, and F. Moglie, "Numerical and experimental analysis of the performance of a reduced surface stirrer for reverberation chambers," in *2012 IEEE International Symposium on Electromagnetic Compatibility*, pp. 156-161, 2012.
[11] J. Clegg, A. C. Marvin, J. F. Dawson and S. J. Porter, "Optimization of stirrer designs in a reverberation chamber," in IEEE Transactions on Electromagnetic Compatibility, vol. 47.4, pp. 824-832, 2005.
[12] H. Huang, X. Chen, M. Li, J. Chen and Q. Li, "Characterization of Stirrer Performance in Reverberation Chamber Using Characteristic Modes," in "2020 14th European Conference on Antennas and Propagation (EuCAP)", pp. 1-4, 2020.
[13] V. Keyser and J. F. Rosnarho, "Criteria of choice of mode stirred reverberation chamber," in *2008 10th International Conference on Electromagnetic Interference and Compatibility*, pp. 267-272, 2008.
[14] A Kenderes, Sz. Gyimóthy, and P. T. Benkő, „On the Field Uniformity of Reverberation Chambers – A Global Sensitivity Analysis Study," in *IGTE Symposium 2022*, submitted for publication.
[15] Marelli, Stefano, and Bruno Sudret, UQLab: A framework for uncertainty quantification in Matlab, American Society of Civil Engineers, 2014.
[16] A. Bingler, S. Bilicz, M. Csörnyei, "Sensitivity Analysis for Automotive EMC Measurements Using Quasistatic Darwin Model," in *COMPEL – The international journal for computation and mathematics in electrical and electronic engineering*, 2021.
[17] A. Bingler, S. Bilicz, and M. Csörnyei, "Polynomial Chaos Kriging Metamodel for Automotive EMC Simulations," in *2022 International Symposium on Electromagnetic Compatibility – EMC Europe*, pp. 873–878, 2022.
[18] Sobol, I.M., "Sensitivity estimates for nonlinear mathematical models," in *Mathematical Modelling and Computational Experiments*, Vol. 1.4, pp. 407-414, 1993.
[19] D. A. Hill, Electromagnetic Fields in Cavities: Deterministic and Statistical Theories, John Wiley & Sons 2009.
[20] Electromagnetic Compatibility (EMC) - Part 4-21: Testing and measurement techniques - Reverberation chamber test methods, IEC 61000-4-21:2011.
[21] F. Monsef, "Why a reverberation chamber works at low modal overlap?," in *IEEE transactions on electromagnetic compatibility*, Vol. 54.6., pp. 1314-1317, 2012.
[22] C. L. Holloway, D. A. Hill, J. M. Ladbury, and G. Koepke, "Requirements for an effective reverberation chamber: Unloaded or loaded," in *IEEE Transactions on Electromagnetic Compatibility*, Vol.48.1, pp. 187-194, IEEE, 2006.
[23] Sudret, B., "Global sensitivity analysis using polynomial chaos expansions," in *Reliability Engineering and System Safety*, Vol. 93.7, pp. 964-979, 2008.
[24] P. S. Palar and K. Shimoyama, "On efficient global optimization via universal Kriging surrogate models," in *Structural and Multidisciplinary Optimization*, Vol. 57.6, pp. 2377–2397, 2018.
[25] R. Schöbi, B. Sudret, and J. Wiart, "Polynomial-chaos-based Kriging," in *International Journal for Uncertainty Quantification*, Vol.5.2, 2015.
[26] Manual, CST Studio Suite Getting Started, CST Studio Suite 2021, Darmstadt, Germany
[27] MIL-STD-461G, Department of Defense Interface Standard: Requirements for the Control of Electromagnetic Interference Characteristics of Subsystems and Equipment, 2015.
[28] S. Wang, Z. C. Wu, G. H. Wei, Y. Z. Cui, L. S. Fan, "A New Method of Evaluating Reverberation Chamber Q-Factor with Experimental Validation," in *Progress In Electromagnetics Research Letters*, Vol. 36, pp.103-112, EMW Publishing, 2013.
[29] A. Bingler, S. Bilicz, and M. Csörnyei, "Global Sensitivity Analysis Using a Kriging Metamodel for EM Design Problems with Functional Outputs," in *IEEE Transactions on Magnetics*, 2022.
[30] A Kenderes, Sz. Gyimóthy, and P. T. Benkő, „On the Field Sensitivity Analysis with Various Parameters in Undermoded Reverberation Chambers," in *COMPUMAG 2023*, digest submitted for publication.
[31] P. Corona, G. Ferrara, and M. Migliaccio, "A spectral approach for the determination of the reverberating chamber quality factor," in *IEEE Transactions on Electromagnetic Compatibility*, vol. 40, no. 2, pp. 145-153, May 1998.